Supporting Information to accompany

Enhancing Redox Functionality in Dinuclear Europium Complexes

Nithin Suryadevara[†], Stanley Bagio[†], Moya A. Hay, Robert W. Gable, and Colette Boskovic*

School of Chemistry, University of Melbourne, Parkville, Victoria 3010, Australia

*c.boskovic@unimelb.edu.au

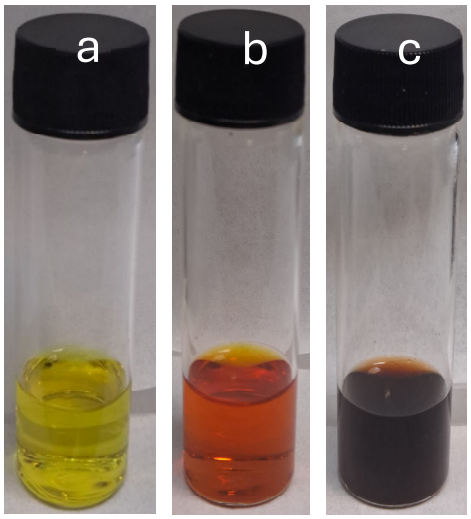

Figure S1. a) EuI_2 in MeCN, b) EuI_2 and tpa in MeCN and c) After addition of bpym ligand solution.

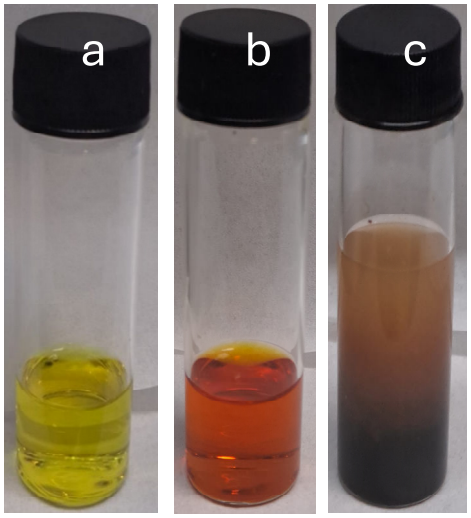

Figure S2. a) EuI_2 in MeCN, b) EuI_2 and tpa in MeCN and c) After layering of bptz ligand solution on top of EuI_2 and tpa mixture

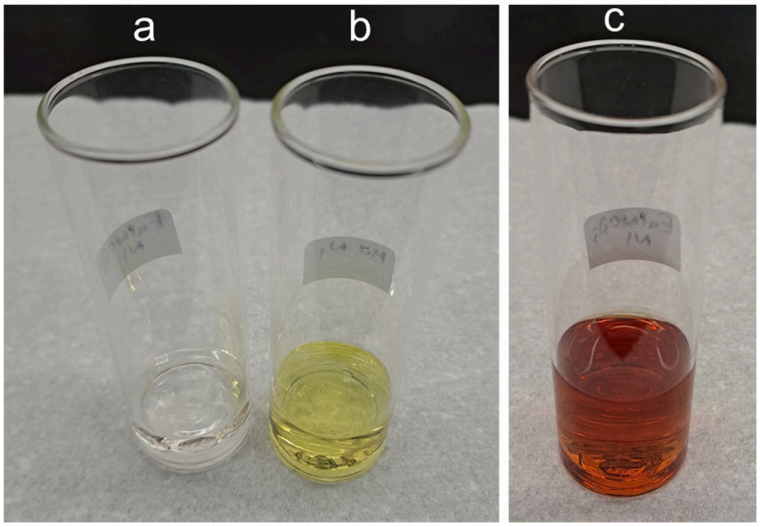

Figure S3. a) $Eu(NO_3)_3 \cdot 6H_2O$ in MeCN, b) Br_4catH_2 and tpa, with triethylamine in MeCN and c) After slow addition of Br_4cat^{2-}/tpa solution into $Eu(NO_3)_3 \cdot 6H_2O$.

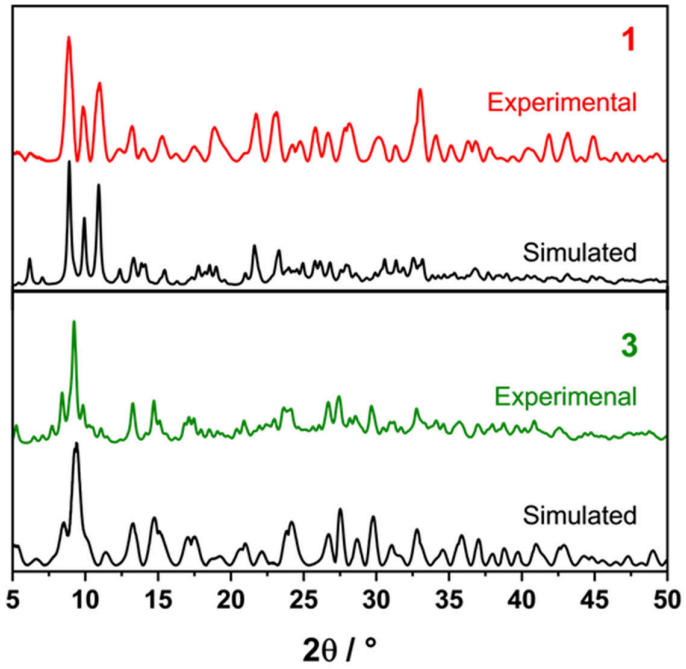

Figure S4. Powder X-ray diffractograms (Cu K_α) for dinuclear **1**·MeCN (top) and **3**·MeCN (bottom)**.** Compared with the simulated data from the crystal structure obtained at 100 K (black).

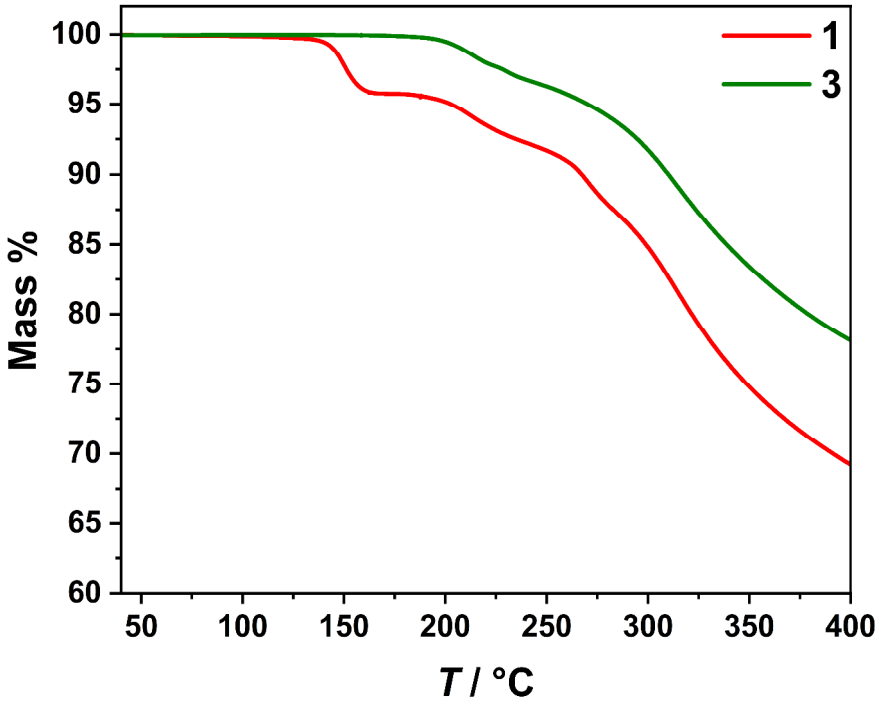

Figure S5. Thermogravimetric analysis plots for **1**·MeCN (red) and **3**·MeCN (green).

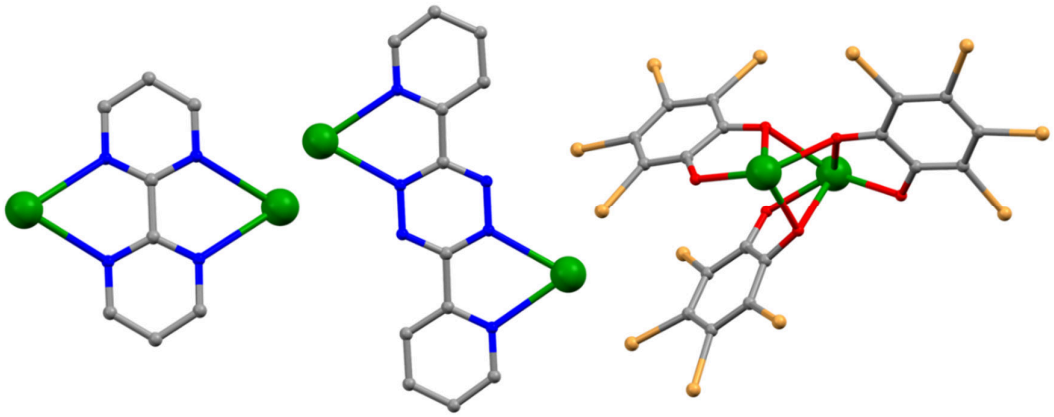

Figure S6. Bridging modes for **1** (left), **2** (middle) and **3** (right).

Table S1: Crystallographic data and structure refinement parameters for **1**·2.5MeCN, **2**·0.7H_2O and **3**·MeCN.

	[(Eu^{II}_2)(I)$_4$(μ-bpym)(tpa)$_2$]·2.5MeCN (**1**·2.5MeCN)	**[(Eu^{III}_2)(I)$_4$(μ-bptz)$^{\bullet-}$(tpa)$_2$][I]** ·0.7H_2O (**2**·0.7H_2O)	**[Eu^{III}_2(μ–Br$_4$cat)$_3$(tpa)$_2$]**·MeCN (**3**·MeCN)
Empirical formula	$C_{44}H_{42}Eu_2I_4N_{12}$ + 2.5[C_2H_3N]	$C_{48}H_{44}Eu_2I_5N_{14}$ + 0.72[H_2O]	$C_{54}H_{36}Br_{12}Eu_2N_8O_6$ + [C_2H_3N]
Formula weight	1653.05	1768.29	2196.80
Temperature (K)	100.01(10)	150.0(2)	100(2)
Crystal system	Triclinic	Orthorhombic	Monoclinic
Space group	*P*-1	*Pbca*	$P2_1/c$
a (Å)	11.7226(4)	20.234(4)	13.799(3)
b (Å)	15.0787(5)	15.617(3)	13.467(3)
c (Å)	16.9543(6)	34.729(7)	34.005(7)
α (°)	104.433(3)	90	90
β (°)	93.699(3)	90	98.47(3)
γ (°)	100.407(3)	90	90
Volume (Å^3)	2835.60(17)	10974(4)	6250(2)
Z	2	8	4
ρ_{calc} (g/cm^3)	1.936	2.141	2.335
μ (mm^{-1})	33.132	5.127	9.717
F(000)	1566	6625.0	4128.0
Crystal size (mm^3)	0.23 × 0.07 × 0.06	0.08 × 0.02 × 0.01	0.08 × 0.08 × 0.06
Radiation	Cu Kα (λ = 1.54184)	Synchrotron (λ = 0.71076)	Synchrotron (λ = 0.71076)
2θ range for data collection (°)	5.418 to 152.778	3.09 to 64.294	2.422 to 64.424
Index ranges	-14 ≤ h ≤ 13, -18 ≤ k ≤ 18, -20 ≤ l ≤ 21	-30 ≤ h ≤ 30, -21 ≤ k ≤ 21, -47 ≤ l ≤ 47	-20 ≤ h ≤ 20, -19 ≤ k ≤ 19, -49 ≤ l ≤ 49
Reflections Collected	29357	193525	109138
Independent reflections	11154	17202	18620
Data/restraints/parameters	11154/0/588	17202/0/636	18620/0/768
Goodness-of-fit on F^2	1.015	1.052	1.109
Final *R* indexes [$I \geq 2\sigma$ (*I*)]	R_1= 0.0512, wR_2= 0.1308	R_1= 0.0396, wR_2= 0.1152	R_1= 0.0281, wR_2= 0.0770
Final *R* indexes [all data]	R_1= 0.0585, wR_2= 0.1365	R_1= 0.0446, wR_2= 0.1789	R_1= 0.0284, wR_2= 0.0772
Largest diff. peak/hole (e Å^{-3})	1.76 / -1.77	2.52/-2.42	2.74/-1.92
CCDC numbers	2420256	2420257	2420258

Table S2: MOS calculations for **3**.

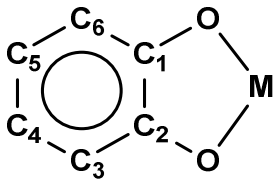

	Avg. C-O	C1-C2	Avg. C2-C3	Avg. C3-C4	C4-C5	MOS
Dioxolene1	1.320	1.431	1.398	1.406	1.384	**-1.67(1)**
Dioxolene2	1.323	1.429	1.394	1.404	1.385	**-1.84(1)**
Dioxolene3	1.314	1.435	1.398	1.406	1.387	**-1.76(1)**

[a] Bondlengths in Å; carbon notations are as per the structure above

Table S3. SHAPE parameters for **1** and **2**.

SHAPE[a]	1	2
SAPR-8	4.2933/3.522	3.045/ 2.991
TDD-8	**2.745**/3.085	**2.481**/**2.616**
JBTPR-8	4.645/3.930	5.404/ 5.433
BTPR-8	3.151/**2.385**	4.097/ 3.936
JSD-8	6.014/6.413	7.145/ 7.215

[a] SAPR-8 - Square antiprism; TDD-8 - Triangular dodecahedron; JBTPR-8 - Biaugmented trigonal prism J50; BTPR-8 - Biaugmented trigonal prism; JSD-8 Snub diphenoid J84

Table S4. SHAPE parameters for **3**.

3a (CN -8)	3b (CN – 9)
7.433 (SAPR-8)	3.576 (JSCAPR-9)
5.057 (TDD-8)	**2.035 (CSAPR-9)**
5.274 (JBTPR-8)	2.739 (JTCTPR-9)
5.038 (BTPR-8)	3.022 (TCTPR-9)
7.096 (JSD-8)	2.345 (MFF-9)

[a] SAPR-8 - Square antiprism; TDD-8 - Triangular dodecahedron; JBTPR-8 - Biaugmented trigonal prism J50; BTPR-8 - Biaugmented trigonal prism; JSD-8 Snub diphenoid J84; JSCAPR-9 - Capped square antiprism J10; CSAPR-9 - Spherical capped square antiprism; JTCTPR-9 -Tricapped trigonal prism J51; TCTPR-9 - Spherical tricapped trigonal prism; MFF-9 - Muffin

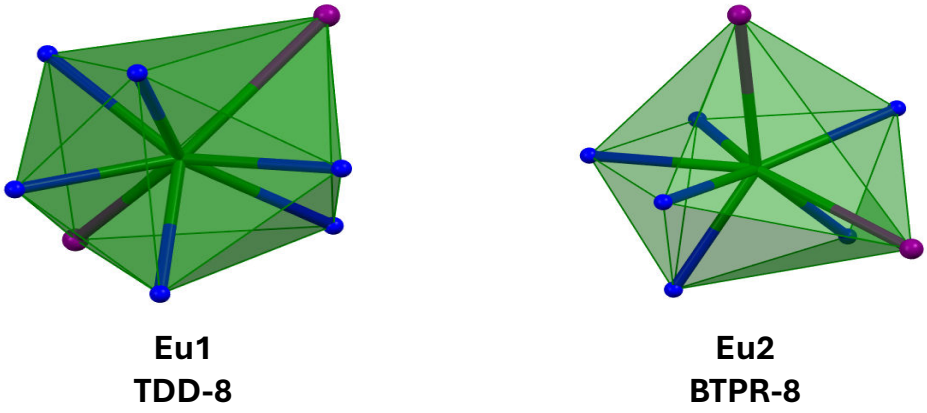

Figure S7. Coordination polyhedra for **1**·2.5MeCN.

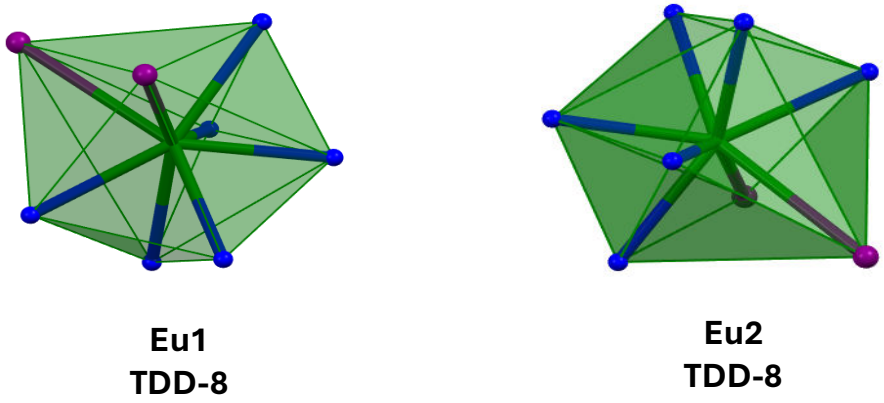

Figure S8. Coordination polyhedra for **2**·0.7H_2O

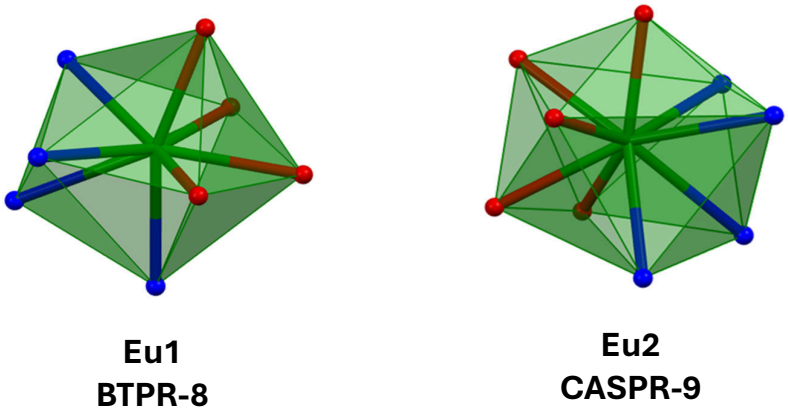

Figure S9. Coordination polyhedra for **3**·MeCN

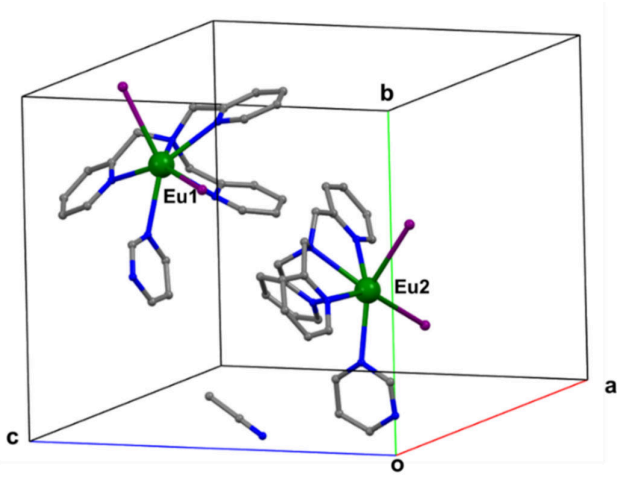

Figure S10. Asymmetric unit for **1**·2.5MeCN.

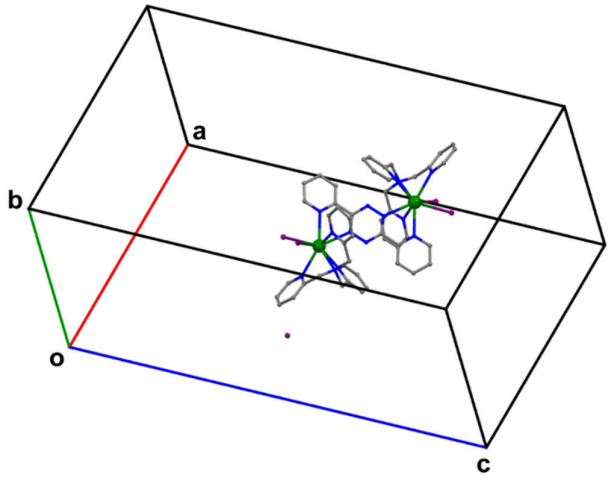

Figure S11. Asymmetric unit for **2**·0.7H_2O.

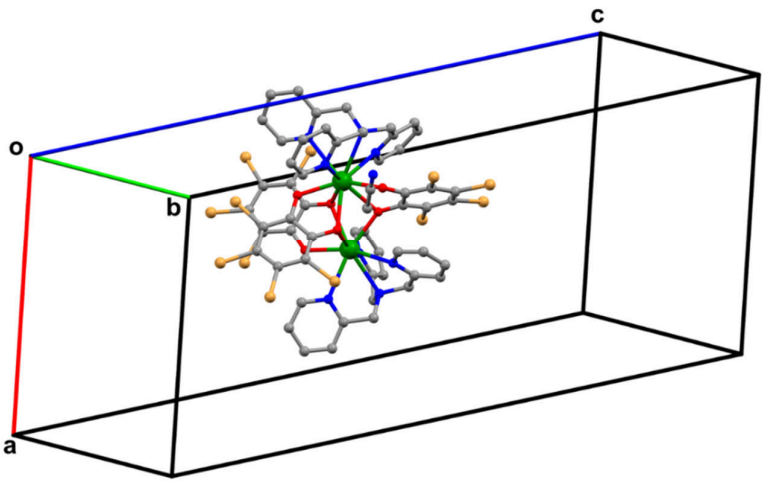

Figure S12. Asymmetric unit for **3**·MeCN.

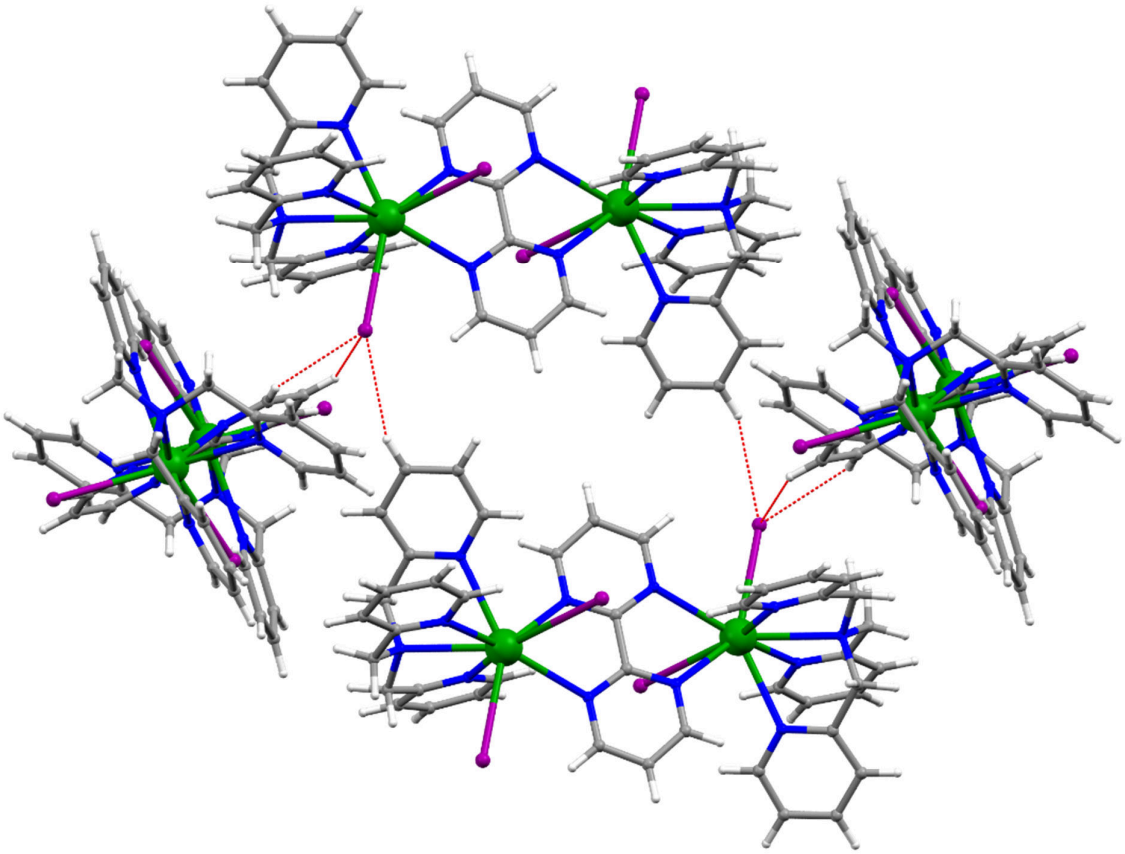

Figure S13. Short intermolecular contacts between molecules 1 and 2 for **1**·2.5MeCN.

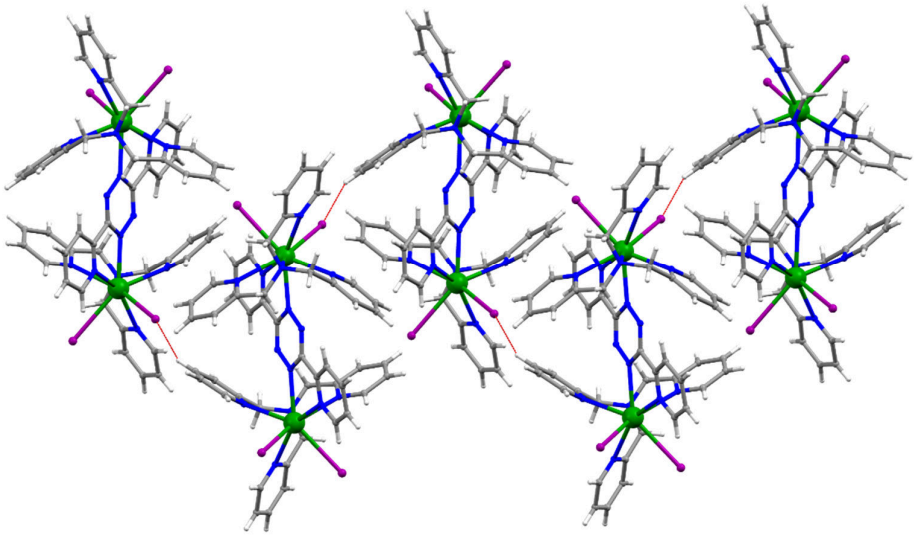

Figure S14. Short contacts for **2**·0.7H_2O**.**

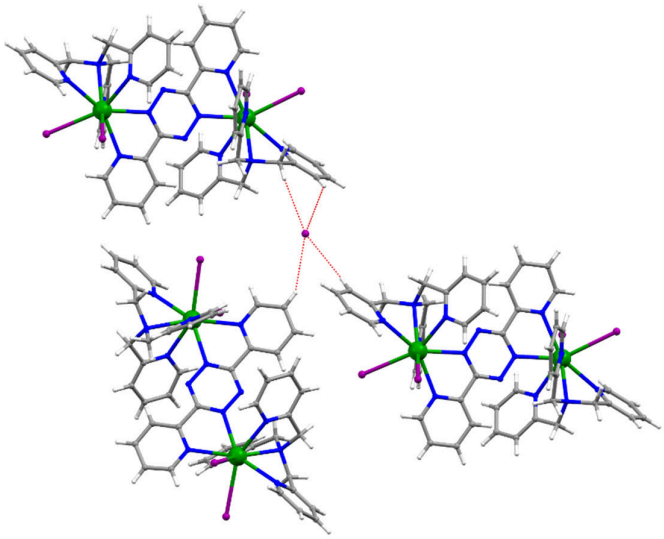

Figure S15. Short intermolecular contacts for **2**·0.7H_2O.

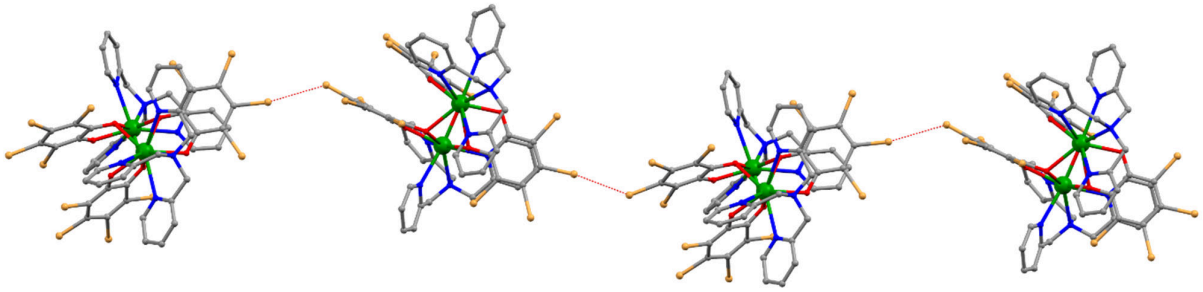

Figure S16. Short contacts for **3**·MeCN (along axis *c*).

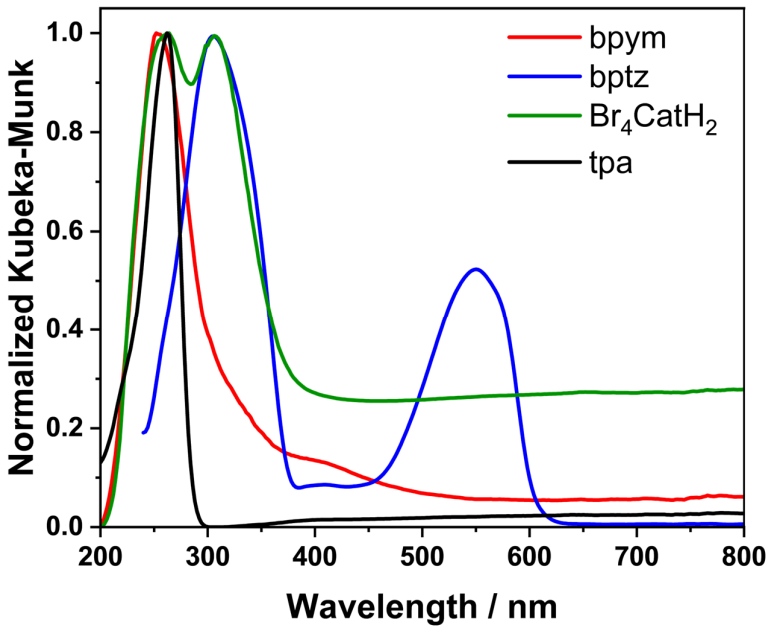

Figure S17. Diffuse reflectance spectra of ligands (bpym, bptz, Br_4catH_2 and tpa)

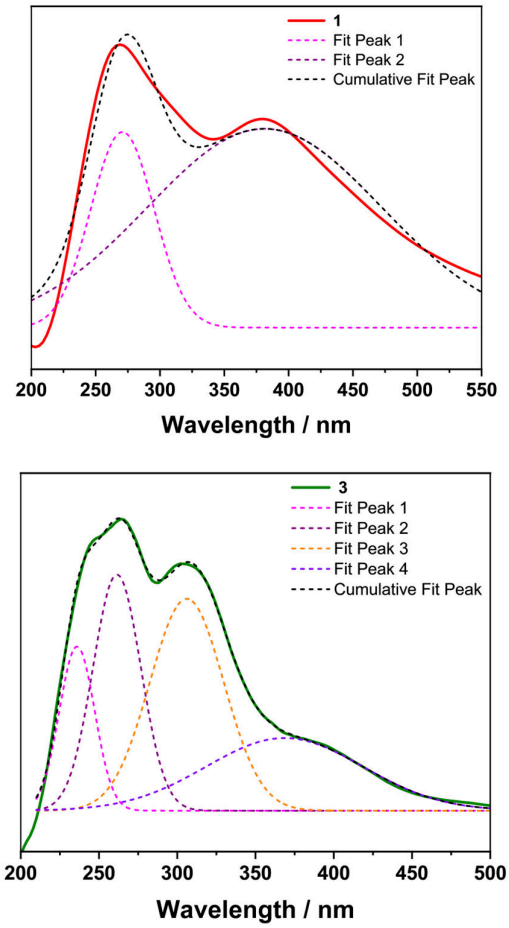

Figure S18. Deconvolution of diffuse reflectance spectra for **1**·MeCN and **3**·MeCN. Spectra of **1**·MeCN with two peak Gaussian fit (R^2 = 0.969) and the spectra of **3**·MeCN was four peak Gaussian fit (R^2 = 0.999).

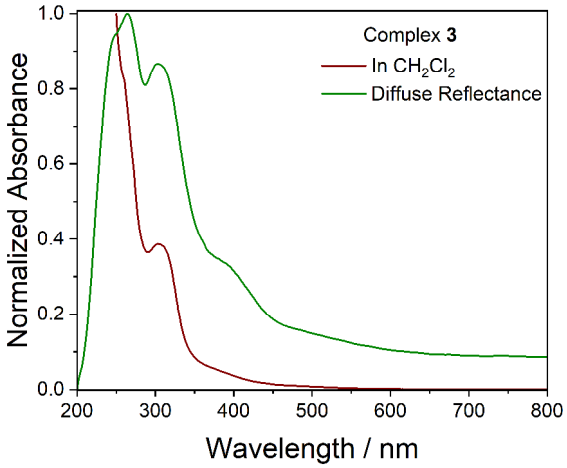

Figure S19. Electronic spectra for **3** in CH_2Cl_2 and in solid state (diffuse reflectance).

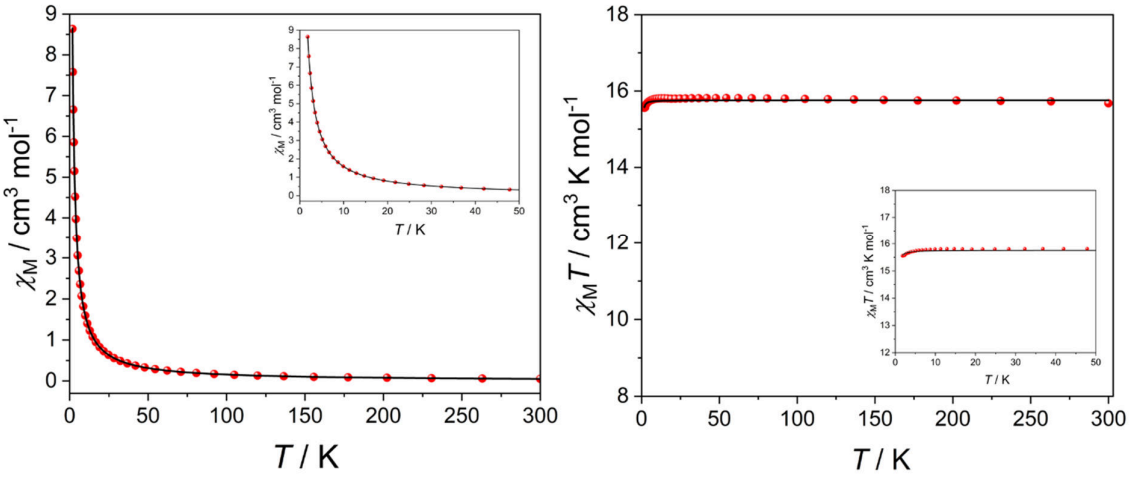

Figure S20. χ_M *vs T* (left) and $\chi_M T$ *vs T* (right) of **1**·MeCN (red) in the range of 1.8–300 K. Data (black line) were fit with software PHI as described in the text. Inset shows the data in the low temperature region (2-50 K).

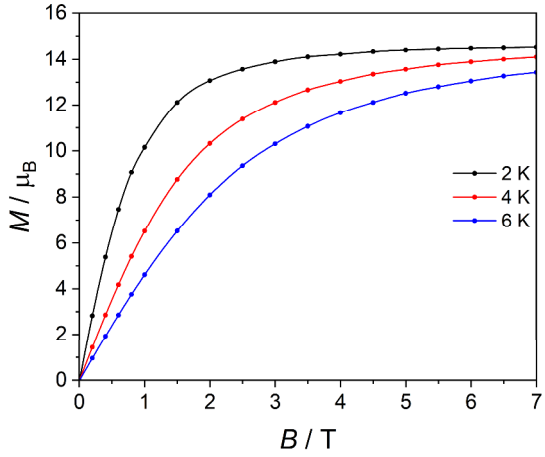

Figure S21. Magnetization versus field data for **1**·MeCN at 2, 4 and 6 K.

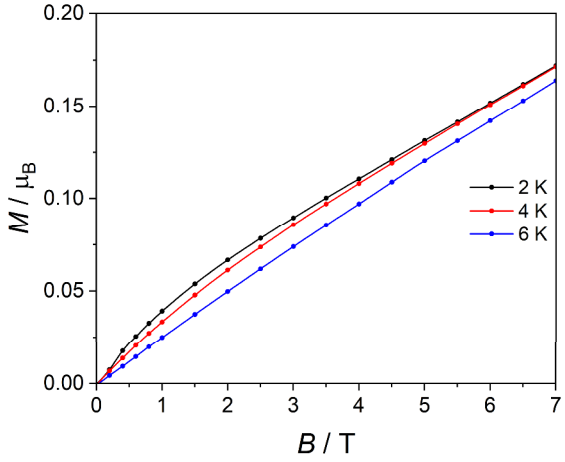

Figure S22. Magnetization versus field data for **3**·MeCN at 2, 4 and 6 K**.**

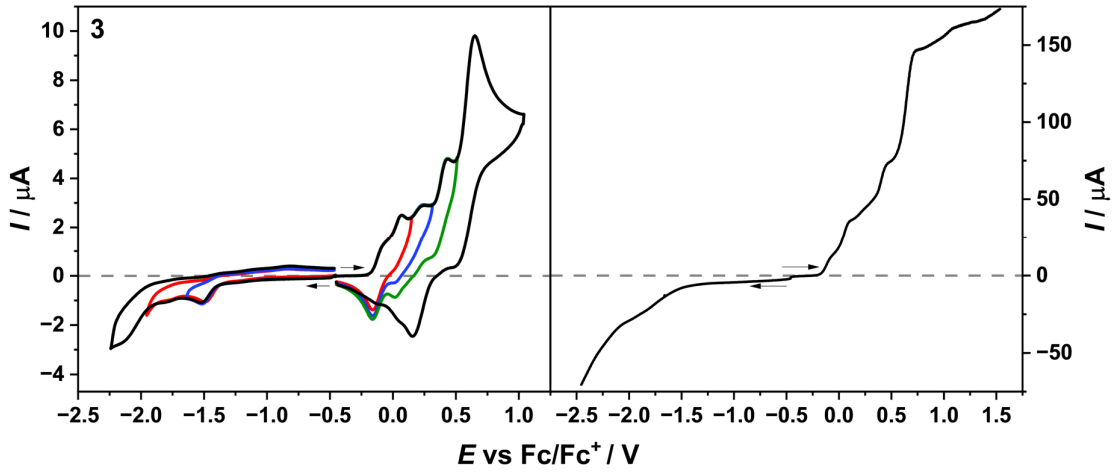

Figure S23. Voltammograms of compound **3** in CH_2Cl_2 (1.0 mM with 0.25 M $TBAPF_6$) obtained with a scan rate of 100 mV s^{-1}. Left: Cyclic voltammogram. Right: Corresponding RDE voltammograms with a rotation rate of 500 rotations min^{-1}. Arrows indicate the starting point and direction of the scan.